Microreactor coating with Au/Al2O3 catalyst for gas-phase partial oxidation of ethanol: Physico-chemical characterization and evaluation of catalytic properties

Behravesh, Erfan; Eränen, Kari; Kumar, Narendra; Peltonen, Janne; Peurla, Markus; Aho, Atte; Nurmi, Maristiina; Toivakka, Martti; Murzin, Dmitry; Salmi, Tapio

Published in:
Chemical Engineering Journal

DOI:
10.1016/j.cej.2019.122179

Published: 01/01/2019

Document Version
Accepted author manuscript

Document License
CC BY-NC-ND

Microreactor Coating with Au/Al_2O_3 Catalyst for Gas-Phase Partial Oxidation of Ethanol: Physico-Chemical Characterization and Evaluation of Catalytic Properties

Erfan Behravesh [a], Kari Eränen [a], Narendra Kumar [a], Janne Peltonen [b], Markus Peurla [c], Atte Aho [a], Mari Nurmi [d], Martti Toivakka [d], Dmitry Yu. Murzin* [a], Tapio Salmi [a]

[a] *Laboratory of Industrial Chemistry and Reaction Engineering, Johan Gadolin Process Chemistry Centre, Åbo Akademi University, FI-20500, Turku/Åbo, Finland*
[b] *Laboratory of Industrial Physics, Department of Physics and Astronomy, University of Turku, FI-20014, Turku/Åbo, Finland*
[c] *Laboratory of Electron Microscopy, University of Turku, FI-20520, Turku, Åbo, Finland*
[d] *Laboratory of Paper Coating and Converting, Johan Gadolin Process Chemistry Centre, Åbo Akademi University, FI-20500, Turku/Åbo, Finland*

*Corresponding author: dmurzin@abo.fi

Abstract

A straightforward and reliable method was successfully developed for stainless steel microreactor coating. The importance of this coating method lies in using an already pre-prepared Au/Al_2O_3 catalyst without incorporation of any binders, addressing the importance of the interplay between the catalyst particle size and slurry viscosity in optimization of the uniformity, stability and thickness of the coating layers. The catalyst and the coated microplatelets were characterized thoroughly using nitrogen adsorption, X-ray Diffraction, Fourier Transform Infrared Spectroscopy, Scanning Electron Microscopy, confocal microscopy, laser diffraction, viscosity measurements, Transmission Electron Microscopy, Energy-dispersive X-ray, Inductively Coupled Plasma-Optical Emission Spectrometry and X-ray Photoelectron Spectroscopy. Moreover, stability of the coating layers was assessed in gas phase partial oxidation of ethanol. Initial increase in the catalyst activity with time on stream was likely due to changes in the gold oxidation state while minor catalyst deactivation could mainly be correlated with coking.

Keywords: Microreactor coating, binder, catalyst particle size, viscosity, gold catalyst, ethanol oxidation

1. Introduction

Application of microreactors is associated with process intensification meaning a reduction in equipment size by several orders of magnitude, thus causing a remarkable decrease in capital and energy costs and a positive environmental impact [1-3]. The commonly known advantages of microscale reactor technology are related to a high surface-area-to-volume ratio (because of thin channels), enhanced heat and mass transfer [4-6] and straightforward scale-up, because conventional scale-up is replaced by number-up [7]: a sufficient production volume is obtained by coupling microscale units in parallel. One of the big advantages of microreaction technology is inherent safety [8] giving lower amounts of industrial wastes and allowing production of hazardous chemicals [9, 10]. The extreme limits of chemistry can be approached by use of microreactors, and operation close to or even within explosion limits is proposed. Moreover, microreactors are efficient tools for the rapid extraction of accurate intrinsic kinetic information [11, 12] which is necessary for scale-up from the laboratory to pilot and full scale production. This is because only small amounts of chemicals and materials are needed and experiments can be performed rapidly in parallel screening devices. Several books and review articles have been published discussing the advantages and the challenges of using microreactors [1, 13, 14] as well as their practical applications [15-20]. Microreactors are extensively used for oxidation reactions, especially selective oxidation of primary and secondary alcohols to the corresponding aldehydes, ketones and carboxylic acids being thus of relevance in organic synthesis practiced in alimentary and pharmaceutical industries [21-23]. Previously, in another work by the authors it was shown that Au/Al_2O_3 catalyst has a high activity and selectivity towards acetaldehyde and ethyl acetate in comparison with some other Au supported oxides and zeolites [24].

One of the most demanding tasks in using microreactors hindering their widespread application is attachment of the catalytically active phase on the walls of the very low volume microchannels [25,

26]. There are important considerations to be made when dealing with microreactor coating such as the catalyst layer uniformity, stability and thickness [27] which should be optimized simultaneously. The uniformity of the layer is the most challenging task because it depends on several factors such as the catalyst particle size, size distribution and viscosity of the catalyst slurry. Moreover, geometry of a microreactor is very crucial in determining the final shape of the catalyst layer as well as providing isothermal conditions within the channels [28]. The layers should also be stable in the reaction conditions; the adhesion of the catalyst layer to the microreactor platelets is usually improved by e.g., the platelets pretreatment such as thermal [29], chemical [30] and anodic oxidation [31]. Additionally, the coating method should be flexible for adjustment of the layers thickness. This task is crucial since the catalytic layer thickness strongly influences the heat and mass transfer and consequently, the performance of the microreactor [32].

Depending on the catalyst, e.g., oxides or zeolites, and the microchannel dimensions, various methods for microreactor coating have been developed such as suspension, sol-gel deposition, hybrid method, electrophoretic and electrochemical deposition, impregnation, physical and chemical vapor deposition, cathodic sputtering, pulsed laser deposition, flame assisted vapor and flame spray deposition, powder plasma spraying, etc. [33]. However, for using metal modified catalysts usually wash coating is applied [34-38] meaning that first the microplatelets are coated with the catalyst support and then the metal nanoparticles are deposited into the meso/micropores of the support material. This approach is suitable, for instance, for achieving more stable catalyst layers since in the absence of metal nanoparticles the support material can be calcined at higher temperatures, while on the other hand, it is not applicable for coating using an already pre-prepared metal modified support.

Moreover, coating is often carried out by using organic binders to improve the adhesion of the support layer. It is noteworthy, that binders can change the morphology of the final product as well

[39] even if e.g., they are burnt out. Moreover, binders could also block the active phase reducing the surface area of the catalyst [40] and application of binders makes the chemistry involved in the catalyst slurry preparation more complex.

Therefore, in the current work a straightforward and reliable method was developed for applying a ready-to-use gold modified alumina catalyst not requiring any additional binders, while preserving crystallinity of alumina. This was done by taking advantage of the interplay between the catalyst particle size and viscosity of the catalyst slurry. Finally, the stability tests of the catalyst layers as well as catalyst durability were carried out for gas phase partial oxidation of ethanol.

2. Experimental section

2.1. Catalyst preparation

In this work, gold was introduced on ɣ-Al_2O_3 (UOP Versal VGL-25) via deposition-precipitation method using hydrogen tetrachloroaurate (III) hydrate (99.9 %-Au) (49 % Au) (chloroauric acid) (Alfa Aesar and ABCR GmbH) as a precursor. 4.73 g dried ɣ-Al_2O_3 was mixed with 400 ml distilled water and stirred vigorously for three hours, thereafter, the mixture was heated up to 70°C. 170 ml of 1.15 g/l gold containing solution was then added to the mixture. The pH at this step was 4.4. The pH of the alumina-gold solution mixture was adjusted to 8 by adding 0.5 ml ammonium hydroxide (NH_4OH) solution 32% (Merck) dropwise as a precipitating agent. The final pH after three hours stirring raised to 8.5. The reason for such an increase in the pH could be due to formation of $AlOH_2^+$ at 70°C [41]. These hydroxide species can facilitate the loss of water from the support, which involves proton consumption and consequently increase the pH. Finally, to remove the chlorine species, the catalyst was filtered and washed with 3 l distilled water followed by drying at 100°C for few hours and calcination in air at 300°C.

2.2. Catalyst slurry preparation for coating

The coating of the microchannels was carried out via the suspension method based on which the slurry of the ready to use catalyst is directly deposited into the microplatelet channels. 5 wt% (solid content) catalyst slurry was prepared by dissolving alumina in distilled water without using any additives. The slurry was stirred at around 300 rpm using a magnetic stirrer for 4 h at 40°C and afterwards at ambient temperature up to four days.

2.3. Microreactor platelet pretreatment, coating and adhesion tests

The microplatelets were thermally treated at 750°C for 3 h with the heating rate of 3°C/min prior to coating. This pretreatment usually leads to the formation of an oxide layer on the stainless steel plates acting as anchoring sites for a better adhesion of the catalyst on the channel walls.

In order to deposit the catalyst slurry into the channels, a 0.5-10 µl Finnpipette was used. 3.5 µl slurry was deposited into the channels of each microplatelet and the excess slurry was wiped off. The plates were dried both at 6°C and room temperature. Finally, the plates were calcined at 300°C. Calcination at higher temperatures was avoided due to probability of the gold nanoparticles sintering. The mass of the catalyst deposited into the channels was measured by weighing the microplatelets before and after the catalyst coating.

Adhesion of the catalyst layer within the plates was tested by subjecting the plates to a rapid nitrogen flow for 5 min as well as exposition for 3 h to ultrasound. The stability of the catalyst layers within the channels was also tested under the reaction conditions during the catalyst durability studies.

2.4. Catalyst powder, catalyst slurry and microplatelet characterization

The characterizations of the catalyst, catalyst slurry and the microplatelets were carried out using nitrogen adsorption, X-ray Diffraction (XRD), Fourier Transform Infrared Spectroscopy (FTIR), Scanning Electron Microscopy (SEM), confocal white light microscopy, laser diffraction, viscosity measurements, Transmission Electron Microscopy (TEM), Energy-disperse X-ray (EDX), Inductively Coupled Plasma-Optical Emission Spectroscopy (ICP-OES) and X-ray Photoelectron Spectroscopy (XPS).

In order to determine the specific surface area and the mesopore volume of as received and the dried catalyst slurry, nitrogen adsorption was utilized (Sorptometer 1900, Carlo Erba Instruments). Prior to the analysis, the catalyst was outgassed for 3 h at 150°C to remove air and moisture from the pores. BET equation was used for the surface area calculations while the pore volume was calculated using the Dollimore-Heal method [42].

The crystallinity structure of the neat γ-alumina, as received gold modified alumina catalyst and the dried aged catalyst slurry was studied using XRD (PANalytical Empyrean X-ray powder diffractometer). The diffractometer was operated in Bragg-Brentano diffraction mode, and the monochromatized Cu-Kα radiation (λ = 1.541874 Å) was generated with a voltage of 45 kV and a current of 40 mA. The primary X-ray beam was collimated with a fixed 0.25° divergence slit, a fixed 10 mm mask, a fixed 1° anti-scatter slit, and a 0.02 rad soller slit. A 7.5 mm anti-scatter slit and a 0.02 rad soller slit was used in the diffracted beam side prior to the proportional counter. The measured 2θ angle range was 5.0-70.0°, with a step size of 0.013° and measurement time of 80 s per step. The samples were ground gently before the measurements to minimize the preferred crystal orientation. The samples were measured on single crystal silicon sample holders. The phase detection limit of the X-ray powder diffraction measurement was limited to approximately 5 %. The measured diffractograms were analyzed with Philips X'Pert HighScore and MAUD programs. HighScore together with MAUD was used for the phase analysis and MAUD for the Rietveld refinement. The Powder Diffraction database and Inorganic Crystal Structure Database (ICSD) were used as sources of reference [43, 44].

Acidity of as received and the dried catalyst slurry was measured using FTIR (ATI Mattson). The Brønsted and Lewis acid sites were determined qualitatively and quantitatively using pyridine (≥99.5%) as the probe molecule. The samples were pelletized to a thin disc and prior to the measurement pretreated at 450°C for 1 h. Thereafter, temperature was decreased to 100°C and

pyridine was adsorbed on the catalysts for 30 min and desorbed subsequently by evacuation at 250, 350 and 450°C, respectively. Desorption of pyridine at 250-350°C corresponds to weak, medium and strong sites, 350-450°C is related to medium and strong sites while the desorption at 450°C reflects the strong sites only [45]. The intensities of spectral bands, 1545 and 1450 cm^{-1}, correspond to Brønsted and Lewis acid sites, respectively. The amount of the Brønsted and Lewis acid sites were evaluated with the aid of molar extinction coefficients reported by Emeis [46].

Scanning Electron Microscopy (Zeiss Leo Gemini 1530) was used to measure the catalyst particle size and to study the homogeneity, thickness and the catalyst layer stability inside the microchannels. The cross-section photos of the microplatelets were taken by Jeol JXA-8530F field emission electron probe microanalyser. The pictures were made with 5kV acceleration voltage. The probe current was 500pA. Beside SEM microphotographs, 2D and 3D microplatelet channel profiles were obtained using a confocal white light microscope (NanoFocus μSurf) to study homogeneity and thickness of the catalyst layers. The particle size measurements were carried out using a Malvern Mastersizer 3000 laser diffractometer. The measured samples were dispersed in distilled water using a Hydro EV wet sample dispersion unit.

The rheology measurements were performed using Physica MCR 300 Rheometer (Anton Paar) with a concentric cylinder CC27. The viscosity measured was a ramp viscosity in a shear rate from 0.01 to 1000 rpm and back. The samples were first sheared at 0.01 rpm, and then the shear was increased to 1000 rpm and reduced again to 0.01 rpm. All the measurements were conducted at room temperature.

Electron microphotographs of the as received and the spent catalyst were obtained with a JEM 1400 Plus Transmission Electron Microscope with 120 kV acceleration voltage and resolution of 0.38 nm equipped with OSIS Quemesa 11 Mpix bottom mounted digital camera. The average particle size distribution was obtained by counting at least 100 particles.

The gold content of the as received catalyst, aged catalyst slurry, spent catalyst, as well as the elemental analysis of the stainless steel microplatelets before and after the thermal treatment was evaluated by EDX (LEO Gemini 1530 with a Thermo Scientific UltraDry Silicon Drift Detector). Magnification of the images corresponded to a Polaroid 545 print with the image size of 8.9 x 11.4 cm. Furthermore, ICP analysis of the as received catalyst was also performed to compare with the measured value using EDX. For ICP-OES, argon plasma was used to excite optical emission of the elements to be analyzed.

XPS was conducted to reveal the oxidation state of Au. The spectra were collected with a Kratos Axis Ultra DLD electron spectrometer using monochromatized Al-K_α source operated at 120 W. The analyser pass energy of 160 eV for acquiring wide spectra and a pass energy of 20 eV for individual photoelectron lines were used. The surface potential was stabilized by the spectrometer charge neutralization system. The binding energy (BE) scale was referenced to the C 1s line of aliphatic carbon, set at 285.0 eV. Processing of the spectra was accomplished with the Kratos software. Powder sample for the analysis was gently hand-pressed into a pellet directly on a sample holder using a clean Ni spatula.

2.5. Experimental setup and catalytic test

The microreactor was purchased from Institute für Mikrotechnik Mainz GmbH (IMM) containing 10 etched stainless steel microplatelets (size 9.5 × 9.5 mm). Each microplatelet had 9 microchannels as shown in Figure 1. The microreactor consisted of 10 stack mixing plates (size 7.4 × 7.4 mm) having 9 curved channels with different radii in order to keep the volume in the channels constant. The gases are mixed in the diffusion chamber before entering the catalyst zone. Two cylindrical cartridges were used to heat up the microreactor. Temperature was controlled by

a PID controller (CalControls 9500P) with a thermocouple in the housing of the microreactor (with ± 1°C accuracy). More details about the microreactor used in this work are presented in Table 1 [40].

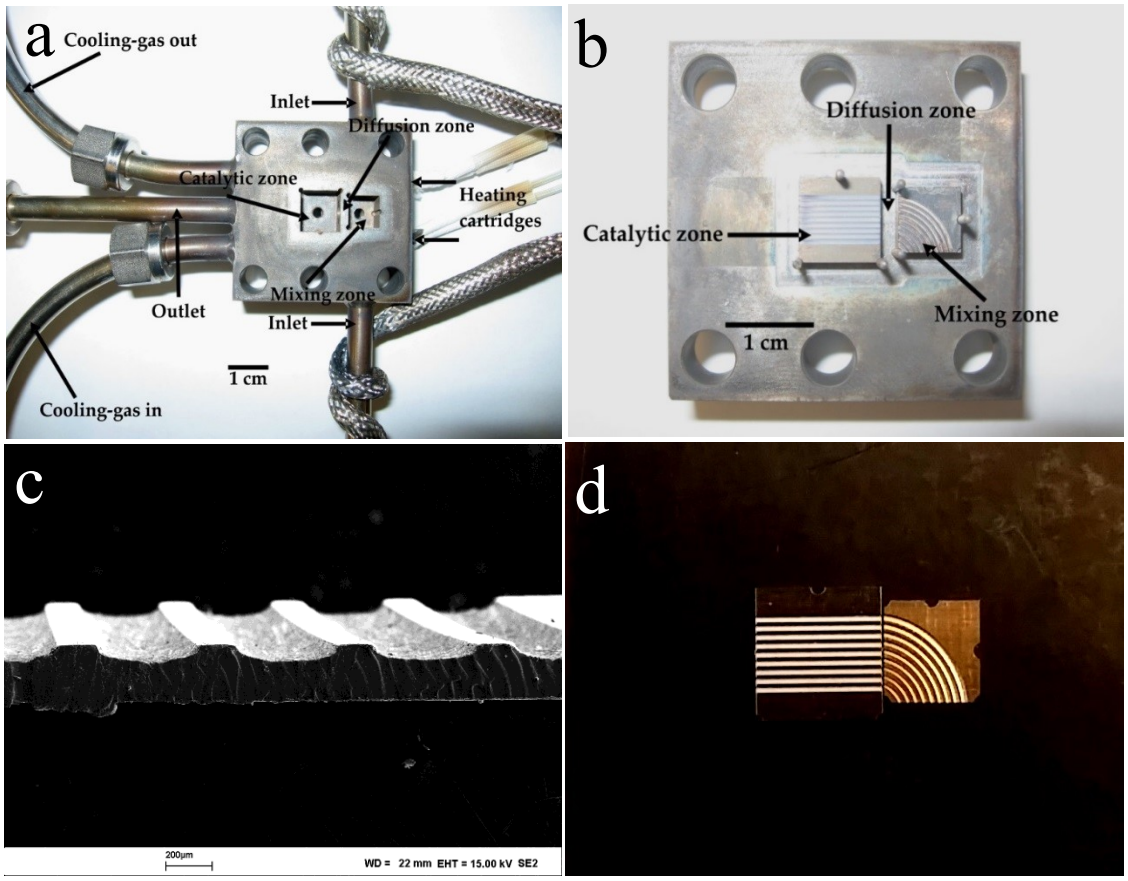

Figure 1. a) Microreactor body, b) mixing, diffusion and catalytic zone, c) cross section of a microplatelet and d) a mixing and a micro plate

Table 1. Technical data of the microreactor used in this work

Property	Value
Model	GPMR-MIX
Size (L x B x H) (mm)	45 × 45 × 32
Connectors (inlet/outlet)	1/4”
Standard material	Inconell 600 (2.4816) for housing and top plate; 1.4571 for mixing and catalyst plates
Number of mixing plates	10
size of mixing plates (mm)	7.5 × 7.5
Channel geometry of mixing plates (width × depth; μm)	180−490 × ∼100
Number of catalyst plates	10
Size of catalyst plate (mm)	9.5 × 9.5
Channel geometry of the catalyst plates (width × depth; μm)	460 × 90
Number of channels per plate	9

The catalytic tests were conducted at atmospheric pressure. A schematic view of the experimental setup is illustrated in Figure 2. The gas mixture contained ethanol, oxygen and helium. Liquid ethanol was fed at room temperature by a HPLC pump (Shimadzu, LC-20AD) to a preheater. The oxygen and helium flows were controlled by Bronkhorst (HIGH-TECH) mass flow controllers. The gas mixture was heated at 100°C prior to the reactor inlet. The total flow rate, the molar ratios and the space velocity (defined as the total flow divided by the overall volume of channels) at the reactor inlet were 100 ml/min, EtOH/O_2/He: 1/3/5.5, and 170,000 h^{-1}, respectively. For the structure sensitivity studies in a fixed bed tubular reactor, a mixture of EtOH/O_2/He with the molar ratio of 1/3/10.2 was fed to the heater at 100°C upstream the reactor with the total flow of 150 ml/min. The reaction was conducted in the temperature range of 100-250°C. The reaction temperature was varied from 100 to 250°C stepwise with 25°C intervals. The heating rate was 3°C/min and the dwelling time at each temperature was 2.5 h. The gas mixture at the reactor outlet

was heated at 130°C to prevent condensation and finally analyzed by an on-line gas chromatograph (Agilent Technologies, 7820A) equipped with both thermal conductivity (TCD) and flame ionization (FID) detectors. The capillary column (HP-PLOT/Q) dimensions were 30 m length, 0.53 mm diameter and 40 μm film thickness. In order to reach the steady state, prior to each experiment, the reactive gas mixture was switched for 30 min.

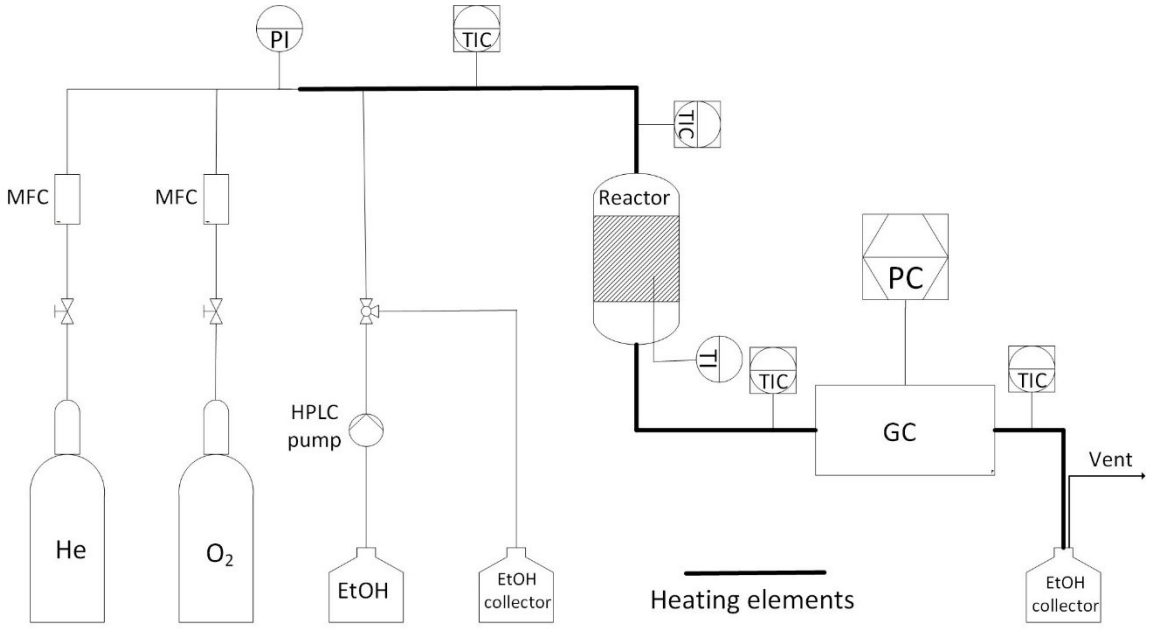

Figure 2. Process flow diagram of the experimental setup where MFC: Mass Flow Controller, HPLC: High Performance Liquid Chromatography, PI: Pressure Indicator, TI: Temperature Indicator, TIC: Temperature Indicator and Controller and PC: Personal Computer

Ethanol conversion (X_{EtOH}), the yield (S) and the product selectivity (Y) were calculated according to the following equations:

$$X_{EtOH} = \frac{C_{Ac} + C_{AA} + 2C_{ETAC} + 2C_{DEE}}{C_{EtOH_0}} \quad (1)$$

$$Y_{ETAC} = \frac{2C_{ETAC}}{C_{EtOH_0}} \quad (2)$$

$$S_{ETAC} = \frac{Y_{ETAC}}{X_{EtOH}} \quad (3)$$

where $C_{EtOH,}$ $C_{Ac,}$ $C_{AA,}$ C_{ETAC} and C_{DEE} stand for the concentration of ethanol, acetaldehyde, acetic acid, ethyl acetate and diethyl ether, respectively, while C_{EtOH_0} is the concentration of ethanol at the reactor inlet.

The turnover frequency was calculated based on the following equation:

$$TOF = \frac{X_{EtOH}.\dot{n}_{EtOH,in}}{n_{Au,tot}.D_{Au}} \quad (4)$$

where X_{EtOH} is the ethanol conversion, $\dot{n}_{EtOH,in}$ is the molar flow of ethanol at reactor inlet, $n_{Au,tot}$ is the total moles of Au and D_{Au} is the Au dispersion calculated based on the following equation [47]:

$$D_{Au} = \frac{6M_{Au}}{a_{Au}\rho N_A d_{vs}} \quad (5)$$

where M_{Au} is the molar mass of gold (0.197 kg mol^{-1}), a_{Au} is the average effective area of a Au atom on the support surface (8.7×10^{-20} m^2), ρ is the density of gold (1.932×10^4 kg m^{-3}), N_A is the Avogadro number and d_{vs} is the volume-surface diameter calculated according to the equation below:

$$d_{vs} = \frac{\sum d_i^{\,3}}{\sum d_i^{\,2}} \quad (6)$$

where d_i is the measured diameter of a gold cluster by TEM.

3. Results and Discussion

3.1. Characterization of the catalyst powder and catalyst coating slurry

3.1.1. Specific surface area and pore volume of the catalyst

The characterization data of the catalyst powder and the catalyst slurry are summarized in Table 2. The specific surface area and the pore specific volume of the pristine and gold modified Al_2O_3 were measured by nitrogen adsorption and calculated based on BET method for the mesopores. The results showed a decrease in surface area and pore volume of γ-Al_2O_3 after gold deposition. The probability of the Al_2O_3 structure distortion in the presence of ammonia (here at pH 8-8.5) during the catalyst preparation is low. In our previous work XRD analysis did not reveal any amorphocity in the structure of the crystalline γ-Al_2O_3 modified with Au at pH 10.5 [24]. Therefore, a decrease in the specific surface area and the pore volume could be due to the presence of Au nanoparticles inside mesopores of alumina. There was no clear difference in the surface area of the catalyst before and after four days of ageing in water. However, a reduction in the pore specific volume was observed. One reason might be due to formation of new phases of alumina such as bayerite precipitating inside the alumina pores known as pore filling [48]. As a result, the surface area reduction could be compensated by the precipitated new phase while decreasing the pore volume.

3.1.2. Au nanoparticle size, dispersion and loading

Characterization of Au including particle size, size distribution and dispersion were done using TEM while the Au loading was measured using both EDX and ICP (Table 2). Figure 3 illustrates the presence of Au nanoparticles on Al_2O_3 exhibiting a very narrow size distribution with an average size of 1.9 nm.

The average Au loading of the as received and the aged catalyst was almost the same implying that the Au nanoparticles were stable on the alumina surface during ageing. Moreover, there was almost

no difference between the loading values measured by EDX and ICP confirming that the average Au loading of the catalyst is about 1 wt%.

Table 2. Characterization data of the catalyst at different steps

Catalyst	Specific surface area (m^2g^{-1})	Pore specific volume (cm^3g^{-1})	Average Au particle size (nm)	Au dispersion (%)	Average Au loading by EDX (wt%)	Average Au loading by ICP (wt%)
γ-Al_2O_3	326	1	—	—	—	—
Au/Al_2O_3 (as received)	308	0.9	1.9	42	0.8	1.2
Au/Al_2O_3 (4 day aged)	314	0.7	—	—	0.9	—

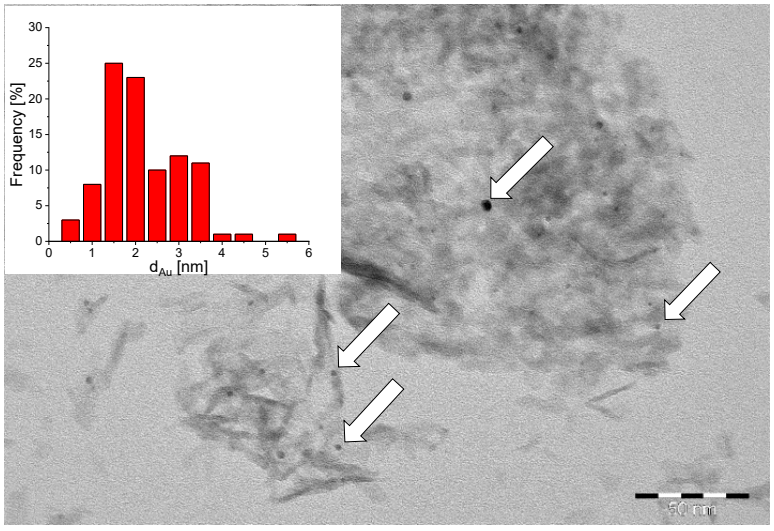

Figure 3. TEM image of Au/Al_2O_3 catalyst showing Au nanoparticles and the particle size distribution

3.1.3. Catalyst particle size

Importance of a small average catalyst particle size and a narrow size distribution for achieving a uniform and stable catalyst layer inside the microchannels is well known [49-52]. Furthermore, small catalyst particle size suppresses the internal diffusion resistance in the catalyst pores. Thus,

the first approach to optimize the coating uniformity is to diminish the catalyst particle size. There are several methods to achieve this goal by for instance, introducing different additives to deagglomerate the particles and overcome attractive forces between the particles. However, additives either for particles deagglomeration or viscosity adjustment such as organic binders could change morphology of the final product [39] or block the pores and diminish the surface area of alumina even if they are e.g., burnt out [40]. Mechanical methods such as milling were also avoided in this work due to their detrimental effects on alumina crystallinity which consequently decrease the surface area of the catalyst. It should be noted that the surface area might even increase after milling [52]; however, changing the physicochemical properties of the catalyst affects the reproducibility of the method. Ultrasonication did not reduce the particle size noticeably either. Another approach is preparation of the catalyst (Au/Al_2O_3) starting from submicronic γ-alumina (20 nm) finally giving a very small catalyst particle size. This approach was also not successful due to formation of larger aggregations (> 50µm) which could not be easily broken. However, unlike other methods, stirring even without using any additive or adjusting pH was a successful approach to deagglomerate the particles. Figure 4 demonstrates that the average catalyst particle size was diminished from 20 to 2 µm after 4 days of stirring in agreement with the scanning electron micrographs (Figure 5).

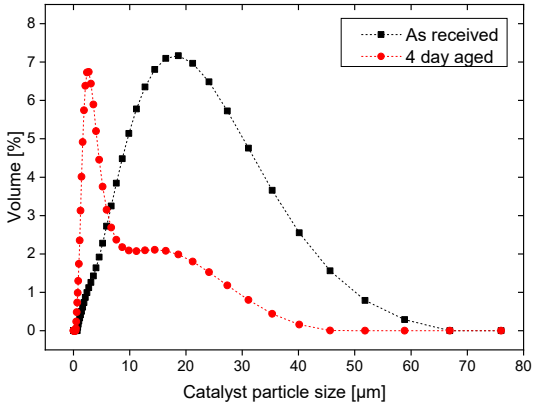

Figure 4. Particle size distribution of the as received and four-day aged catalyst measured by laser diffraction

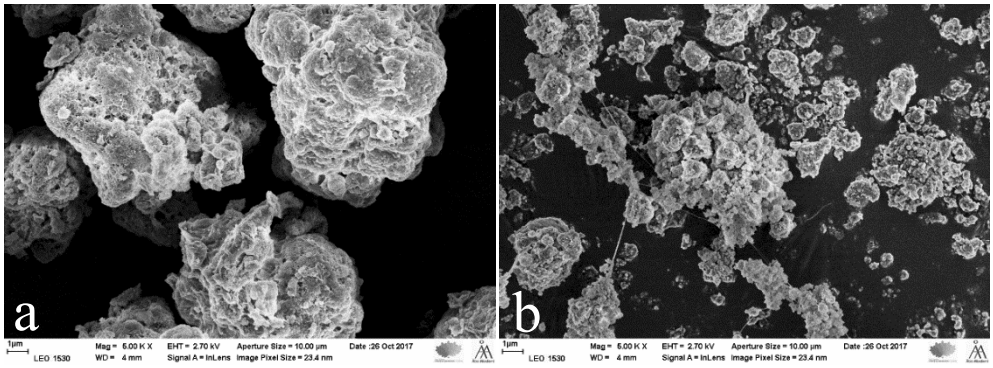

Figure 5. Scanning electron micrographs of the a) as received and b) four-day aged catalyst

This method was more efficient in terms of the particle size reduction than other reported methods in the literature. For instance, in a work conducted by Meille et al. [53] grinding the slurry of alumina-water-nitric acid for one month reduced the average catalyst particle size from 16 to 7 µm. In another study, ageing of alumina slurry with acetic acid and acrylic acid up to 8 days decreased the average particle size noticeably even if the size distribution was still very broad containing very large particles [54]. It should be noted that a bimodal distribution of large and small particles might lead to a higher packing density [39].

3.1.4. pH measurements

Figure 6 illustrates changes in pH over ageing time (Figure 6-a) while temperature of the slurry was adjusted at 45°C for 4 h at the beginning and afterwards at room temperature (Figure 6-b). As it can be seen from Figure 6-a, after 4 h ageing at 45°C there was a steady and slow increase of pH which might be to some extent explained by dissolution of alumina. Zeta potential measurements (not shown here) did not show a clear difference between the surface charge of the catalyst particles

before and after ageing. It should be taken into account that hydration of γ-alumina often occurs via the transformation of alumina surface into aluminum hydroxide which is more prone at pH > 5 when the contact time between alumina and water exceeds 10 h [55]. Thermodynamic calculations have shown that even at neutral pH the alumina is not stable upon contact with water [56]. The calculated free energy of hydration reactions of γ-alumina in water leads to the formation of bayerite ($\Delta G_{298\,k}$ = -1149 kJ/mol) [57], gibbsite ($\Delta G_{298\,k}$= -1154 kJ/mol) [57] and boehmite ($\Delta G_{298\,k}$= -917 kJ/mol) [57]. No new phases of alumina were detected by using nitric acid at pH below 3.5 [53]. In the same studies, the particle size reduction even after one month of grinding was about 50 % of the original particle size which is considerably less efficient compared to 90 % reduction in the current work. In a report of Cristiani et al. [58], a large part of the nitric acid consumption below pH 3.5 was attributed to the dissolution of alumina even if only 1 % of the total alumina was dissolved.

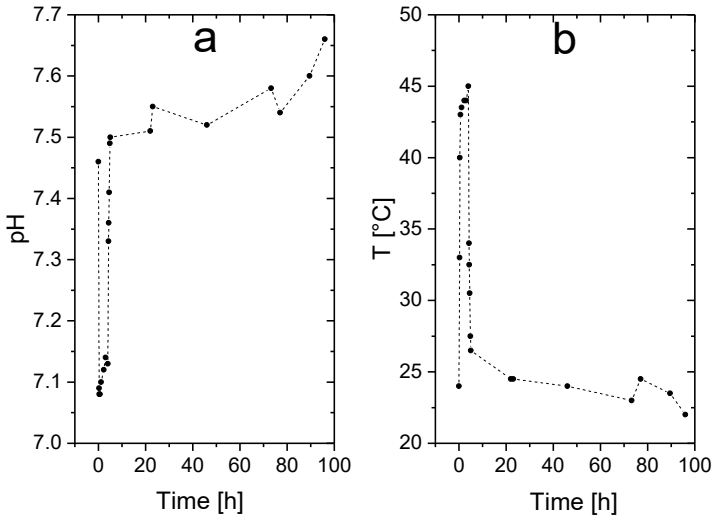

Figure 6. a) Influence of stirring time on catalyst slurry pH and b) temperature monitoring during a four-day stirring process

3.1.5. Acidity measurements

Dissolution of γ-alumina was also investigated by the acidity measurement of the catalyst using FTIR with pyridine as a probe molecule (Table 3). Acidity of the medium and strong sites was too low and could not be measured due to poor resolution of the peaks. The concentration of weak Lewis acid sites of alumina diminished in the presence of water after four days, which might be indicative of Al dissolution. Generally, alteration of ɣ-Al_2O_3 can be explained by either surface hydration through hydrolysis of $Al-O$ bonds or dissolution of alumina and subsequent precipitation [55, 59].

Table 3. Measurement of Brønsted and Lewis acid sites of the as received and four-day aged Au/Al_2O_3 catalyst slurry using FTIR with pyridine

Catalyst	Brønsted acid sites			Lewis acid sites		
	250°C	350°C	450°C	250°C	350°C	450°C
As received	0	0	0	46.8	17.5	0
4 day aged	0	0	0	37.1	not clear	not clear

3.1.6. Structural analysis

In order to examine crystallinity of the catalyst, XRD analysis of the neat γ-alumina, Au modified alumina and the aged catalyst slurry was performed. The diffractograms are demonstrated in Figure 7 together with the reference peaks. The diffraction peaks originating from γ-Al_2O_3 as the reference [60] were observed in the neat γ-Al_2O_3. The peaks were broad, indicating that the crystals are small (Table 4).

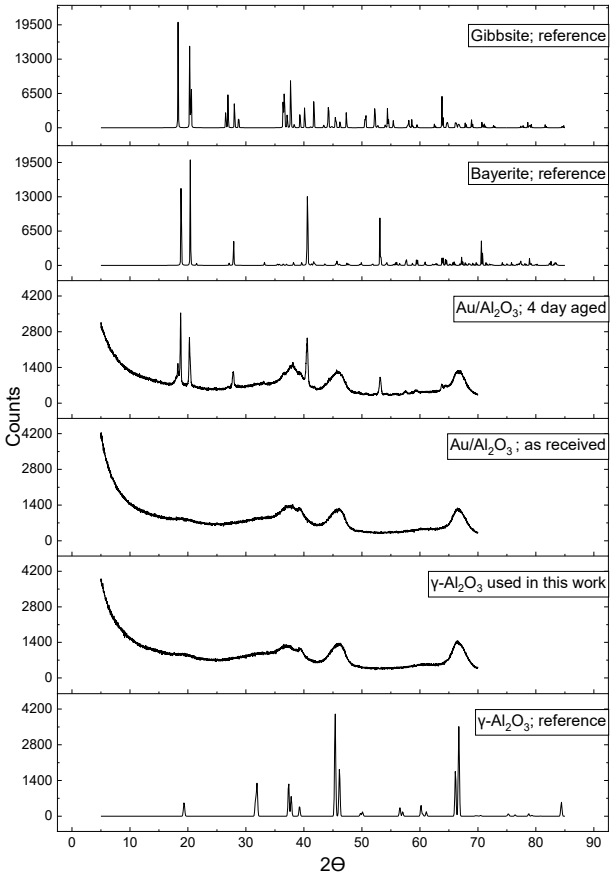

Figure 7. XRD diffractograms of the neat γ-Al_2O_3, as received Au/Al_2O_3 and the four-day aged Au/Al_2O_3 together with gamma alumina, bayerite and gibbsite reference peaks

In diffractogram of the as received Au/Al_2O_3 diffraction peaks originating from γ-Al_2O_3 were observed implying that the diffractogram was practically identical to the previously measured γ-Al_2O_3. These peaks were broad indicating that the crystal size was small.

However, the XRD analysis of the four-day aged catalyst showed that besides the diffraction peaks originating from γ-Al_2O_3, $Al(OH)_3$ bayerite (monoclinic) [61] and $Al(OH)_3$ gibbsite (monoclinic) were also present as the new phases [62] which are usually formed according to the following reaction [56]:

$$Al_2O_3 + 3H_2O \rightarrow 2Al(OH)_3 \quad (7)$$

The corresponding γ-Al_2O_3 peaks were also broad implying that the crystal size was small while the bayerite and gibbsite peaks were narrow and of high intensity. The transformation of γ-Al_2O_3 to the crystalline bayerite after four days of ageing has been also reported in the literature [56].

The Rietveld refinement method was used to estimate the phase weight proportions $w_i/\Sigma w$ and crystal sizes d_c. The quality of the Rietveld refinement fit was described by the parameter R_{exp}, where a smaller R_{exp} indicates a better fit to the measured data. The observed phases, the determined phase weight proportions and crystal sizes are presented in Table 4.

Table 4. The obtained phase weight proportions $w_i/\Sigma w$ and estimated average crystal sizes d_c based on the Rietveld refinements

Sample	Observed phase (framework)	$w_i/\Sigma w$ [%]	d_c [nm]	R_{exp} [%]
γ-Al_2O_3	Al_2O_3 (gamma)	100	3 ± 1	3.28
Au/Al_2O_3 (as received)	Al_2O_3 (gamma)	100	3 ± 1	3.38
Au/Al_2O_3 (4 day aged)	Al_2O_3 (gamma)	82 ± 8	5 ± 2	3.45
	$Al(OH)_3$ (bayerite)	13 ± 4	160 ± 30	3.45
	$Al(OH)_3$ (gibbsite)	5 ± 4	50 ± 20	3.45

As it was discussed before, γ-alumina is thermodynamically an unstable phase and has a high tendency to transform to the other phases in aqueous solutions This was also confirmed here; 13 wt% of the γ-alumina was transformed into bayerite while gibbsite was the minor observed phase, however, the crystallinity of the γ-alumina was preserved.

3.1.7. Viscosity measurements

Besides the particle size distribution, the viscosity of the catalyst slurry plays a crucial role in uniformity of the catalyst layers. Low viscosity causes the slurry to slip down the channel walls leading to formation of much thicker catalyst layer at the bottom than on the walls, whereas high viscosity does not allow the slurry to move along the channels. Therefore, viscosity of the catalyst slurry should be optimized. The viscosity adjustment is usually done for instance by using thickeners, however, in this work, the viscosity was only adjusted by changing the catalyst particle size due to the interplay between the particles size (as well as size distribution) and viscosity [53, 63, 64].

Accordingly, the viscosity of the slurry was measured during ageing (Figure 8). The viscosity measurements were performed with a loop test, in which the shear rate was increased to a certain level and then decreased back to zero. The loop of the four-day aged slurry is demonstrated in Figure 8-a showing that the flow is time-dependent since the two curves did not exactly overlap. A non-Newtonian behavior for all the samples is also evident especially at higher shear rates known as shear thickening behavior implying that the viscosity increased by decreasing the shear rate (Figure 8-b). This observation is in line with the literature where decrease of the viscosity with shear rate was reported for ɣ-Al_2O_3 slurry and suspensions [54, 58, 63].

Furthermore, Figure 8-b also reveals that the viscosity of the slurry increased during ageing. It is noteworthy that viscosity is mainly dependent on pH or particle's zeta potential [63] and the particles shape (crystal morphology) [65]. The pH did not change noticeably during ageing. Neither clear differences in the zeta potential measurements (not shown here) were observed, no SEM images showed any clear changes in the particles shape (shown in supporting information), and no crystallinity distortion of alumina was observed by XRD as discussed above. Therefore, the reason of the viscosity increase can be correlated to a decrease in the particle size. In other words, when the particles become smaller, first, the effective volume fraction increases because the electric

double layer is larger for smaller particles [66] and second, the mean distance between the particles becomes shorter at a given volume fraction increasing the double layer interactions and lowering fluidity [66, 67].

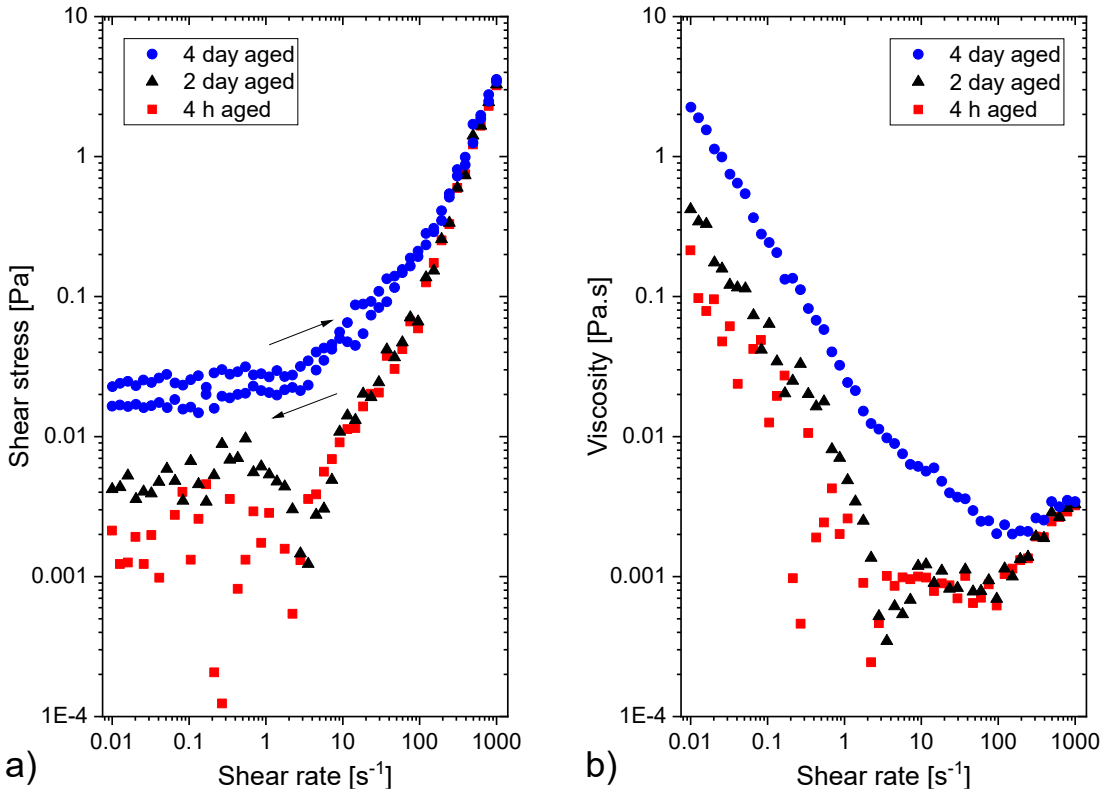

Figure 8. Rheological behavior of the catalyst slurry during 4 days of ageing

3.2. Characterization of the uncoated microplatelets

As the first step, the microplatelets were thermally treated prior to coating by calcining in air at 750°C for 3 h. As Figure 9 illustrates, calcination led to the formation of an oxide layer on the surface of the plate. Quantitative analysis of the oxide layers created by the thermal treatment was performed using EDX (Table 5) showing that 10.5 wt% of the thermally treated stainless steel microplatelet is attributed to oxygen. The oxide layer acts as anchoring sites keeping the catalyst

slurry stable on the channel walls as well as improving the uniformity of the coating layers. The surface roughness of the calcined plates was 0.28 μm calculated from the 3D pictures of the channels taken by a confocal white light microscope. The calculation was the arithmetic average of the surface roughness according to the following equation [40]:

$$S_a = \frac{1}{MN} \times \sum_{k=0}^{M-1} \sum_{l=0}^{N-1} |z(x_k y_l)| \quad (8)$$

where M and N are the number of the positions in *x* and *y* positions, *k* and *l* are indices for position along *M* and *N,* and $|z(x_k y_l)|$ is the vertical deviation at position $x_k y_l$ from the mean line.

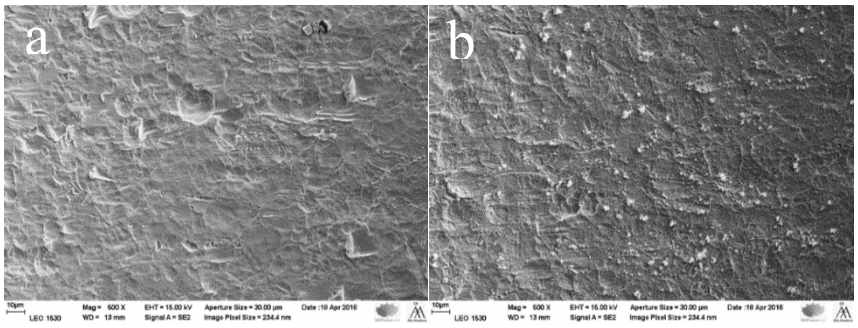

Figure 9. SEM images of a microplatelet a) before and b) after calcination at 750°C

Table 5. Elemental composition of the microplatelet before and after the thermal treatment determined by EDX

Element	As received (wt%)	Pretreated at 750°C (wt%)
Oxygen	0	10.5
Aluminum	0.15	0.25
Silicium	0.64	0.96
Chromium	17.66	18.23
Manganese	2.45	3.16
Iron	67.29	56.73
Nickel	10.11	8.48
Molybdenum	1.68	1.7

3.3. Characterization of the coated microplatelets

3.3.1. Catalyst layer uniformity

The catalyst layer uniformity inside the microchannels was studied by SEM (Figure 10) and confocal microscopy (Figure 11). As Figure 10-a illustrates, whole channels are covered by the catalyst and no severely uncoated areas can be seen. Figure 10-b demonstrates that the catalyst particles stayed on the channel walls and subsequently on the bottom of the channels (Figure 10-c) look very uniform. A close up on the catalyst layer shows only very narrow cracks which are usually formed during drying, however, no sever cracks were observed. The catalyst layer uniformity was also studied by comparing the layer thickness in the middle and the end of the channels using confocal white light microscopy (Figure 11). The maximum difference in thickness was only 1 µm which is mainly due to migration of the catalyst particles towards the end of the channel, as soon as drying starts.

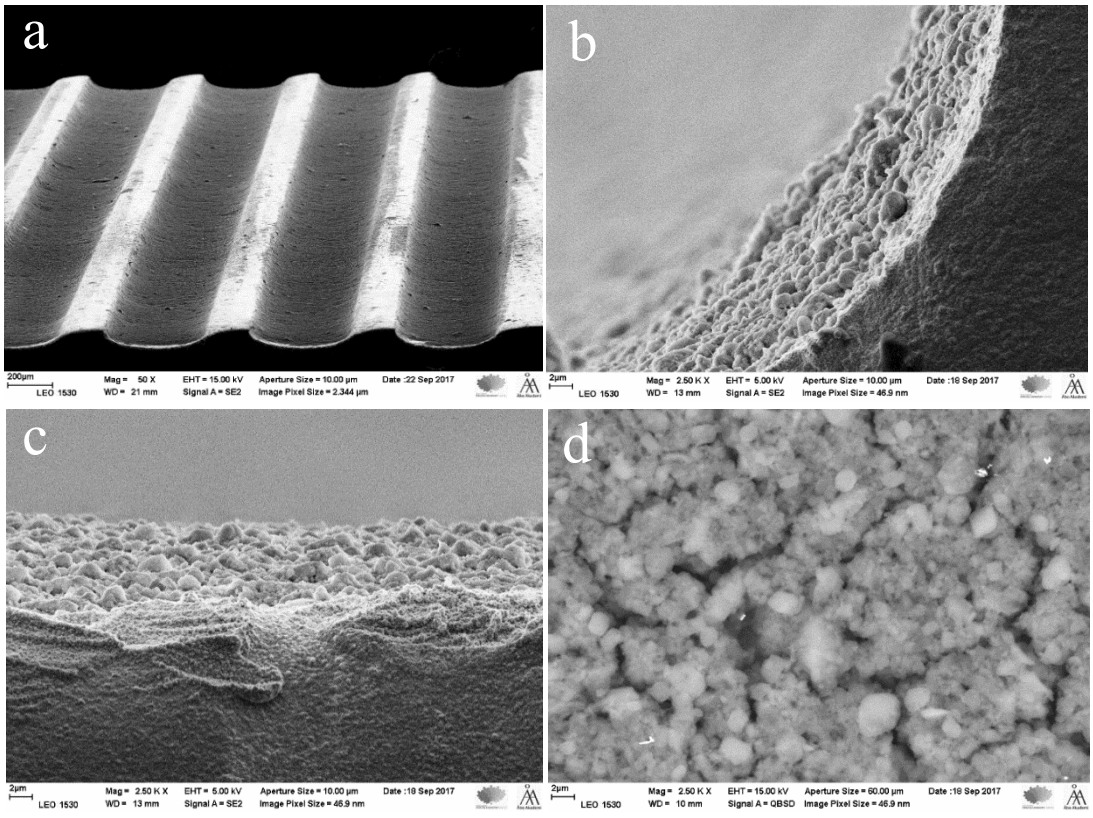

Figure 10. SEM images of a catalyst-coated microplatelet: a) overall view of the channels, b) channel wall, c) bottom of the channel and d) close up on the catalyst layer

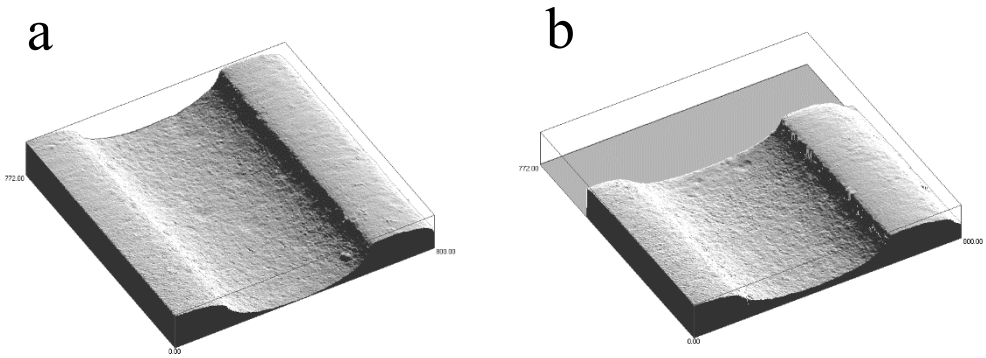

Figure 11. Confocal white light images of a catalyst-coated microplatelet: a) the middle and b) the end of a microchannel

It is noteworthy that the drying rate and temperature play a crucial role in achieving uniform layers. The cracks are usually formed because of thermal stress during drying which might even cause the detachment of the catalyst layers from the microchannels [68]. Thus, the drying rate should be slow enough to prevent ruptures and cracks in the catalyst layer [39]. At the same time presence of some cracks can be beneficial as of both cracks and cavities might enhance diffusion in the layer and might improve the catalyst performance as long as the adhesion and mechanical durability of the layer is preserved [69]. Large cracks, however, also cause channeling inside the catalyst layers.

While Figure 12 does not display a clear difference between the uniformity of the catalyst layers dried at room temperature and 6°C, visual inspection revealed that drying at lower temperature resulted in a more uniform coating.

Herein, in order to lower the drying rate, the microplatelets were dried in a beaker covered by parafilm (Parafilm M, Sigma).

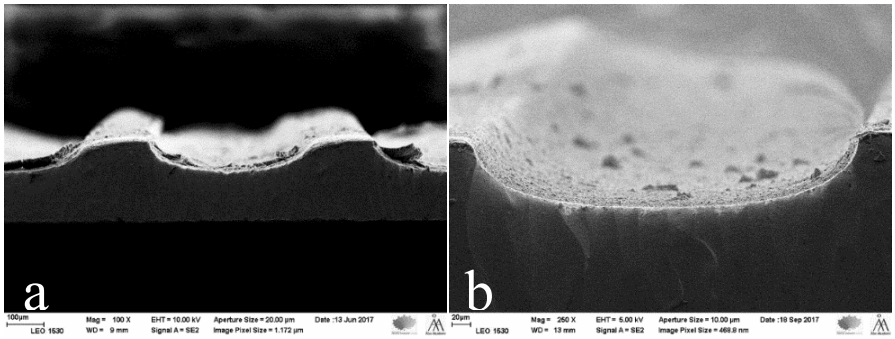

Figure 12. SEM images of a catalyst-coated microplatelet dried at a) room temperature and b) 6°C

Besides the drying rate and temperature, there are other parameters affecting the coating uniformity such as channel dimension (V- versus U-shape profile) [54, 70, 71]. However, there are no general rules for predicting the coating shape by only selecting channel dimensions since also viscosity of the catalyst slurry plays a crucial role in defining the catalyst layer shape within the channels. Herein, a so-called U shape layer profile was observed indicating the presence of slightly more catalyst at the bottom of the channels than on the walls.

3.3.2. Catalyst layer thickness

Adjusting the catalyst layer thickness while optimizing uniformity and stability of the layers is a demanding task which sets new challenges. There are different methods to adjust the catalyst layer thickness within the channels e.g., by multiple layer deposition or changing the viscosity of the

catalyst slurry using additives [30]. However, herein, the thickness was adjusted by changing the slurry volume (2.5-7 µl) while keeping the solid content constant (5 wt%). Table 6 shows a correlation between the slurry volume and the layer thickness. The thickness of the catalyst layer at the bottom of the microchannel was measured from SEM images (Figures 13). The enhancement in the thickness of the catalyst layers was observed with an increase in the volume of the slurry. On the other hand, as Figure 13 illustrates, cracks are more prone in thicker layers of the catalyst even though the dispersion of the catalyst within the channels was uniform. The explanation for the cracks can be due to less interaction between the catalyst particles at the upper part of the thick layers and the surface of the microplates. The microplatelets with 7 µm catalyst layer thickness were thus selected for further studies to prevent potential instability of thicker layers. The corresponding mass of the catalyst on these plates was 1.6 mg (0.16 mg on each plate) which was measured by weighing the plates before and after the slurry deposition.

Table 6. Dependence between 5 wt% catalyst slurry volume in each microplatelet and the coating thickness at the bottom of each channel

Slurry volume (µl)	Coating thickness (µm)
2.5	4.5 ± 0.5
3.5	7 ± 1
5	14 ± 1
7	19 ± 1

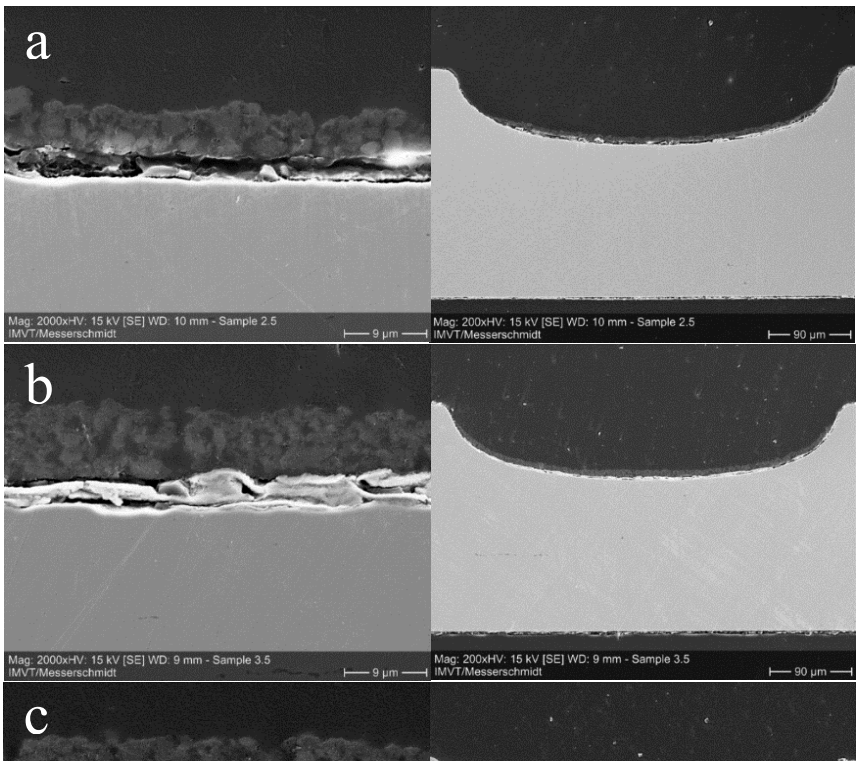

Figure 13. SEM images of the microchannels cross-section coated with: a) 2.5 µl, b) 3.5 µl, c) 5 µl and d) 7 µl catalyst slurry

3.3.3. Catalyst layer stability, catalyst durability and regeneration studies

In order to examine stability of the catalyst layers within the microchannels, the microplatelets were subjected to a rapid nitrogen flow for 5 min as well as exposure to ultrasound for 3 h. As a result, no damage of the catalyst layers was observed by SEM (shown in supporting information) confirming a satisfactory layer stability.

However, the most reliable stability test is using the coated microplatelets under the real reaction conditions. Herein, a reaction test was carried out with the aim of examining stability of the catalyst.

Figure 14 shows conversion, turnover frequency (TOF) and selectivity at different temperatures. As Figure 14-a indicates, the light-off temperature for ethanol oxidation is 175°C and that ethanol conversion of 8 % was achieved at 250°C equivalent to TOF of 0.18 s^{-1}. For calculation of TOF, the reactions taking place only on gold were taken into account excluding e.g., etherification which is assumed to take place on the acidic support surface only. It was previously reported that the main pathway of ethanol oxidation on neat Al_2O_3 is towards diethyl ether formation [24]. Selectivity towards acetaldehyde was 100 % up to 200°C but decreased thereafter because of etherification (Figure 14-b). Selectivity towards diethyl ether was ca. 17 % at 225°C, while esterification took place only at the highest utilized temperature giving selectivity of 4 %. A comparison of selectivity at the same ethanol conversion shows that the main product was acetaldehyde followed by diethyl ether and ethyl acetate (Figure 14-c). Acetic acid, ethylene and CO_2 were not detected.

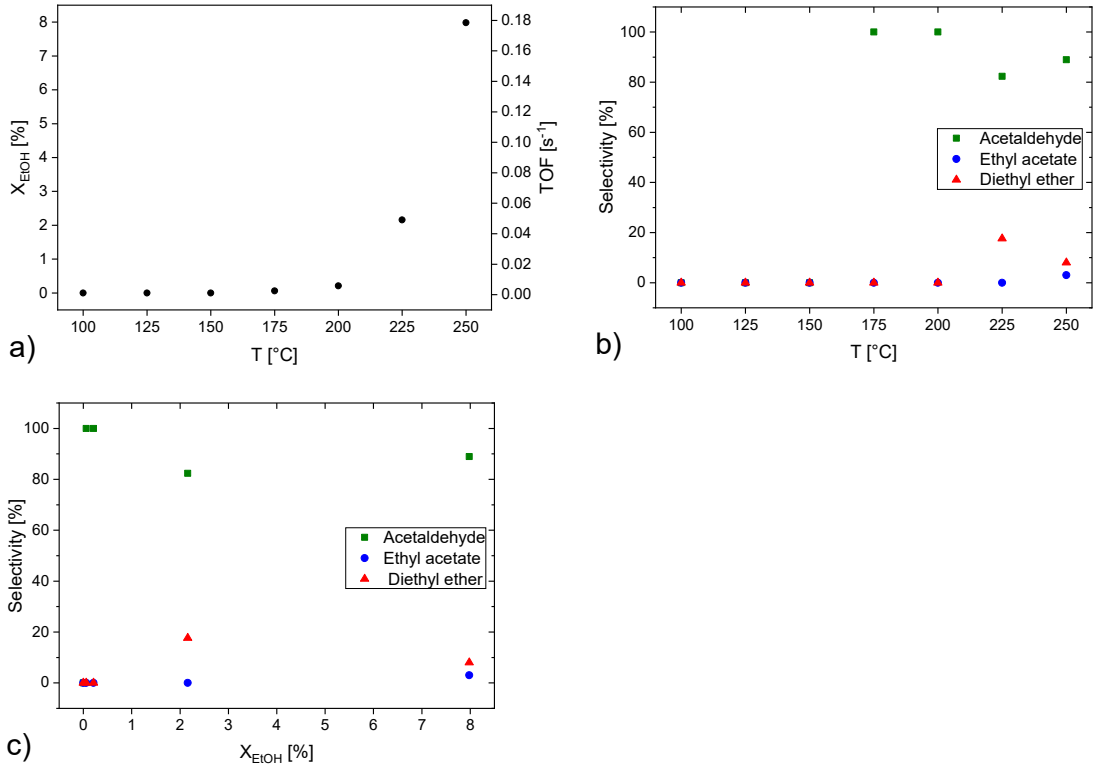

Figure 14. Activity and selectivity of the catalyst in partial oxidation of ethanol in the microreactor at different temperatures

In order to investigate catalyst durability, the reaction test was continued by keeping the temperature constant at 250°C for about 24 days. The results are summarized in Figure 15 showing that the catalyst activity increased at the beginning of the experiments as the ethanol conversion elevated from 8 to about 11 % in 10 h while thereafter, it was rather stable for 90 h (Figure 15-c). Ethanol conversion slowly decreased to 8 % during 273 h.

Selectivity towards acetaldehyde was initially ca. 88 % and decreased to 76 % during 24 days while the ethyl acetate selectivity indicated a minor decrease from 4 to 3 % during the whole test. Etherification was the second dominant reaction which led to formation of diethyl ether giving selectivity of 10 % at the beginning, but increasing to 20 % at the end of the test. There are several reasons for catalyst deactivation including coke formation, sintering of gold nanoparticles and changes in the oxidation state of Au. Coke formation is a very common phenomenon especially for ethanol dehydration over acidic supports being responsible for blockage of the active phase of the catalyst. Therefore, herein, a regeneration experiment was performed to burn out the coke. It is noteworthy that usually due to very small amounts of catalyst in microreactors (here 1.6 mg), detailed physico-chemical characterization, especially surface area measurements, is difficult to perform.

The regeneration was done in-situ by feeding oxygen in helium at 300°C. After 3 h, the oxygen flow was switched off, the temperature was decreased to 250°C followed by feeding of the gas mixture of ethanol, oxygen and helium again into the reactor. As Figure 15-d shows, a lower ethanol conversion (6 %) was unexpectedly observed after the regeneration test, however, it started to rise again and in 15 h it reached 8.5 %, thereafter becoming relatively stable for 250 h. It can be thus speculated, that the activity decrease after the regeneration test is related to the presence of leftover

coke acting as a reducing agent and changing the oxidation state of Au. Due to a very small catalyst amount, quantification of the amount of coke and its nature is very challenging. Therefore, other available techniques were applied to characterize the catalyst layers stability in microplatelets and reveal the reasons for the catalyst deactivation.

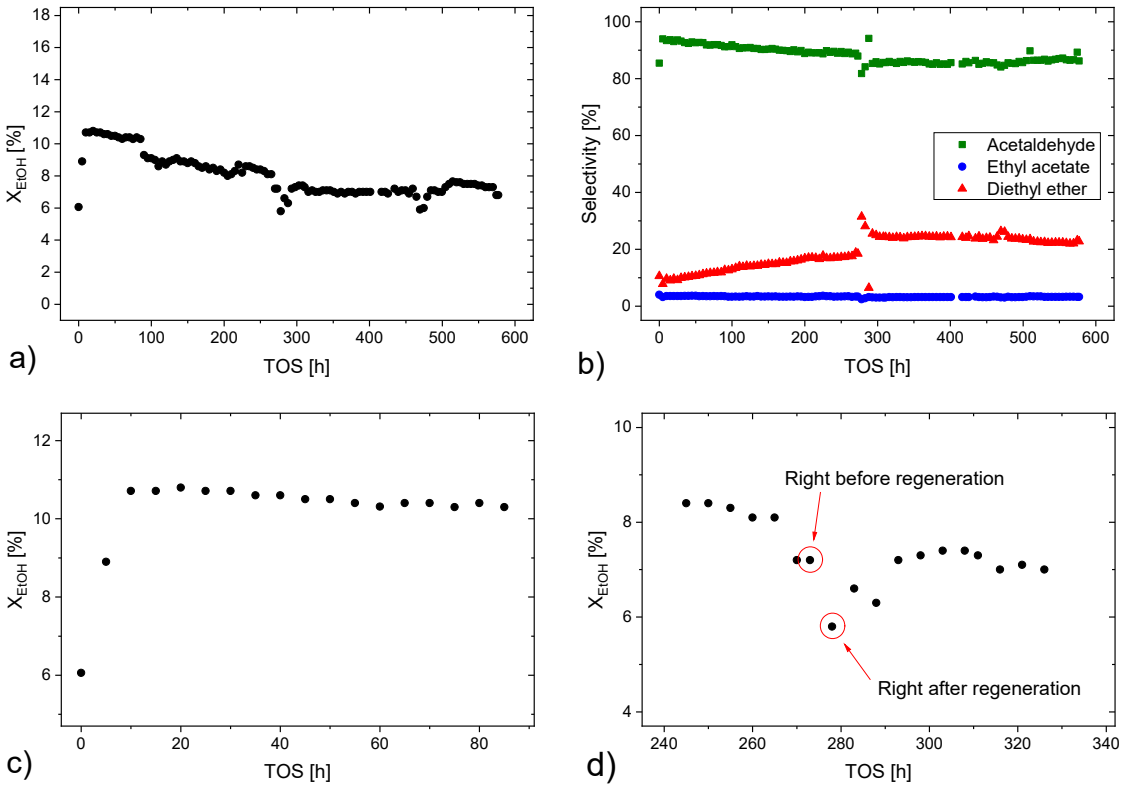

Figure 15. Activity and selectivity of the catalyst during durability studies in the microreactor at 250°C; a) ethanol conversion, b) selectivities, c) conversion at the beginning of the test and d) conversion right after regeneration

SEM images were taken to compare the catalyst coating layers before and after the reaction test (Figure 16). The images did not reveal any damage to the coating layers within the microchannels,

which is a clear indication of the strong interactions between the catalyst coating layer and the microchannels surface, hence, further confirming suitability of the coating method.

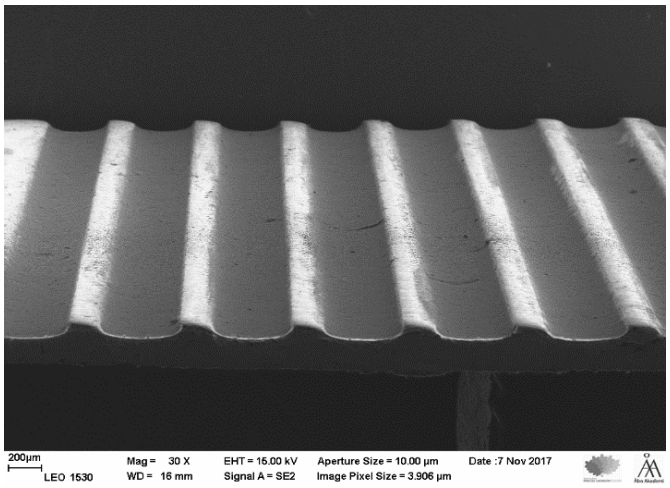

Figure 16. SEM image of a coated microplatelet after the stability/durability test

Table 7 summarizes the characterization results including Au content in the fresh and spent catalyst measured by EDX. Gold content before and after the reaction was essentially the same within an experimental error indicating that Au was strongly attached to alumina.

The oxidation state of Au in the spent catalyst was measured by XPS. A very weak and scattered signal for Au4f was recorded (Figure 17). This in addition to inferior signal-to-nose ratio does not allow unequivocal interpretation of the results. Nevertheless, location of $Au4f_{7/2}$ at 83.6 eV

according to the literature data corresponds to the metallic state of gold Au^0 [72]. Moreover, no other chemical states of gold were detected. In our previous study [24] Au/Al_2O_3 catalysts prepared using the same protocol as the present catalyst had a binding energy of 83.8-84 eV which is in the range of the metallic state. These results indicate that the oxidation state of Au did not change after the reaction, indicating strong interactions between Au^0 and Al_2O_3.

Table 7. Characterization results of the catalyst before and after long-term stability test

Catalyst	Au average cluster size (nm)	Au dispersion (%)	Au loading by EDX (wt%)	Au loading by ICP (wt%)	Au oxidation state ($4f_{7/2}$) (eV)
Fresh	1.9	42	0.8	1.2	—
Spent	2.8	35	1	—	83.6

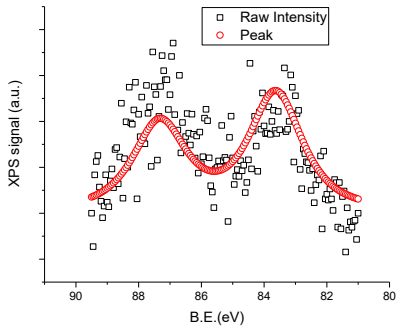

Figure 17. XPS spectrum of spent Au/Al_2O_3 catalyst

A slight increase in the average Au particle size from 1.9 to 2.8 nm was observed in TEM images implying that sintering of the Au nanoparticles might have occurred which consequently led to lower Au dispersion (Figure 18). However, the particle size distribution was almost within the same range as for the fresh catalyst. In order to confirm whether sintering of Au nanoparticles was responsible for a decrease in catalyst activity, structure sensitivity studies were performed using a fixed bed tubular reactor keeping the $EtOH/O_2$ molar ratio constant. In order to have a fair comparison of TOF for Au particles, the contribution of reactions processing on alumina, namely esterification and etherification, was subtracted from TOF calculations. As Figure 19 illustrates, the level of TOF values was higher than in the microreactor which can be related to a lower conversion level in the microreactor.

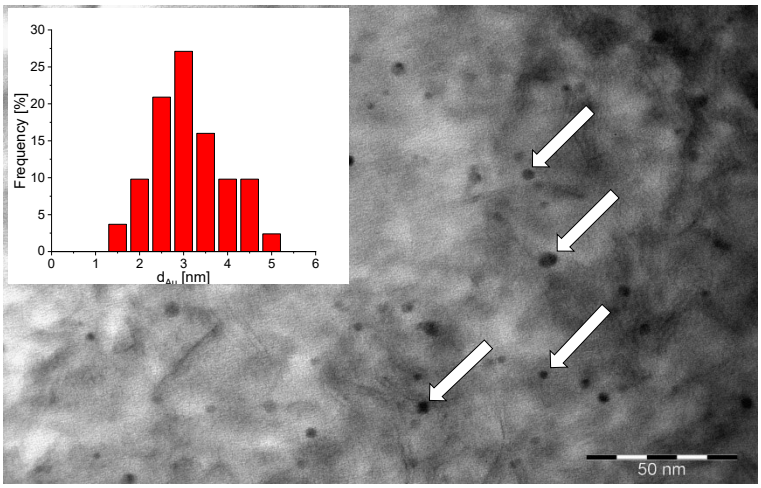

Figure 18. TEM image of the spent catalyst and gold particle size distribution

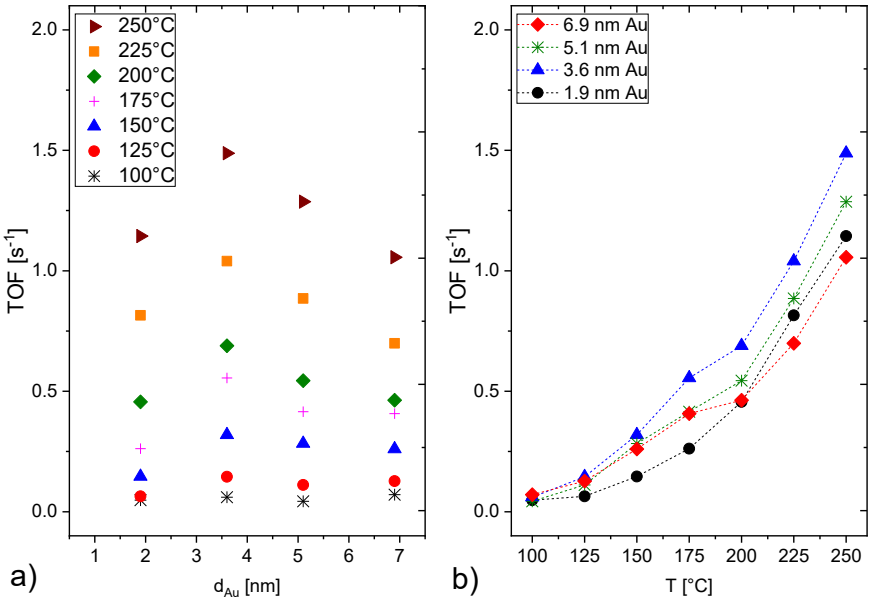

Figure 19. TOF of ethanol oxidation on Au/Al_2O_3 catalysts with different gold particle sizes in a fixed bed reactor

Lower TOF for 1.9 nm Au compared to 3.6 nm is also observed which is more pronounced at higher temperatures. This could be attributed to the fact that small gold particles having mainly edge and corner atoms exhibit lower catalytic activity, thus the presence of face atoms on the surfaces of Au particles is more crucial for catalysis. As Figure 19 clearly indicates, the optimum gold particle size is estimated to be between 1.9 and 3.6 nm which means that Au nanoparticles sintering leading to an increase in the average gold particle size from 1.9 to 2.8 nm, should have resulted in an increase in the catalyst activity rather than deactivation. A rather fast increase in the catalyst activity has also been reported in the literature for Au/Al_2O_3 in ethanol oxidation, although in the liquid phase [73].

Summarizing, the main reason of catalyst deactivation could not be attributed to the metal particles sintering but can mainly be related to coke formation.

Unlike the catalyst deactivation, an increase in the catalyst activity was observed at the beginning of the durability test (Figure 15-c). In order to confirm this activation, another set of experiments was conducted using fresh coated microplatelets in consecutive cycles (increasing and decreasing the temperature with the same ramp) in the temperature range of 100-250°C. The ethanol conversion during heating and cooling at 150°C is shown in Figure 20. During the ascending stage, ethanol conversion in the first cycle started from zero and after the third cycle it was elevated to a slightly higher level, indicating some catalyst activation. A reason for this activation can be changes in the Au oxidation state which later on might have been reduced again by coke acting as reducing agent.

Moreover, it can be seen from Figure 20 that conversion is always higher during descending in all cycles compared to the corresponding ascending path. In the second cycle, the conversion started again from zero although it was higher in descending in the first cycle. This can be correlated to local overheating of the active sites of the catalyst [74] which means that the actual temperature of the gold particles exceeds that of surroundings. Accordingly, the measured temperature of the catalyst bed decreases while the temperature of the active phase lags behind. As the last cycle indicates, ca. 10 h was required for the catalyst to approach the same conversion level as displayed during the ascending route. After the seventh cycle the catalyst activity remained relatively constant demonstrating almost steady state activity in the whole temperature range.

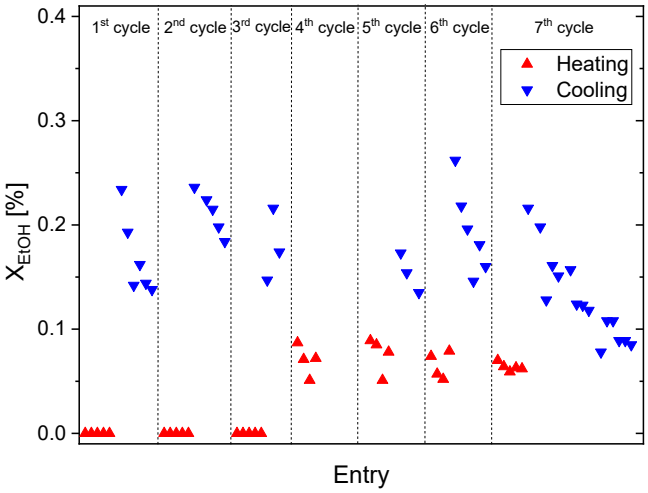

Figure 20. Ethanol conversion in consecutive cycles at 150°C; the time interval of the values is 30 minutes

3.4. Reproducibility tests of the catalytic behaviour after the slurry preparation

It is important to examine whether the catalyst after the slurry preparation exhibits similar catalytic behaviour under the reaction conditions. Therefore, both the as received and the dried slurry were tested in the reactor; because the as received catalyst could not be used in the microreactor due to its large particle size (20 μm on average), both catalysts were tested in the fixed bed reactor to compare the performances. The reactor had 1 cm inner diameter and was packed with 160 mg of the catalyst giving the bed height of 1.5 cm. The reaction conditions were the same as for the microreactor. Prior to the reactor packing, the dried aged catalyst was gently crushed to break the agglomerates which were formed during evaporation of water from the slurry.

Figure 21 shows the ethanol conversion and selectivity within the temperature range of 100-250°C. Unlike the microreactor, acetic acid was observed which can be related to very different residence time (ca. 25 times shorter in the microreactor). A small increase and decrease in

acetaldehyde and diethyl ether selectivity, respectively, could be correlated to the slight dissolution/transformation of alumina as discussed above. On the other hand, slight changes in the catalytic performance might also originate from deviations in the reactor packing and analytical precision. In any case, the aforementioned changes are minor meaning that even slight alumina dissolution/transformation did not have a clear effect on the catalyst performance.

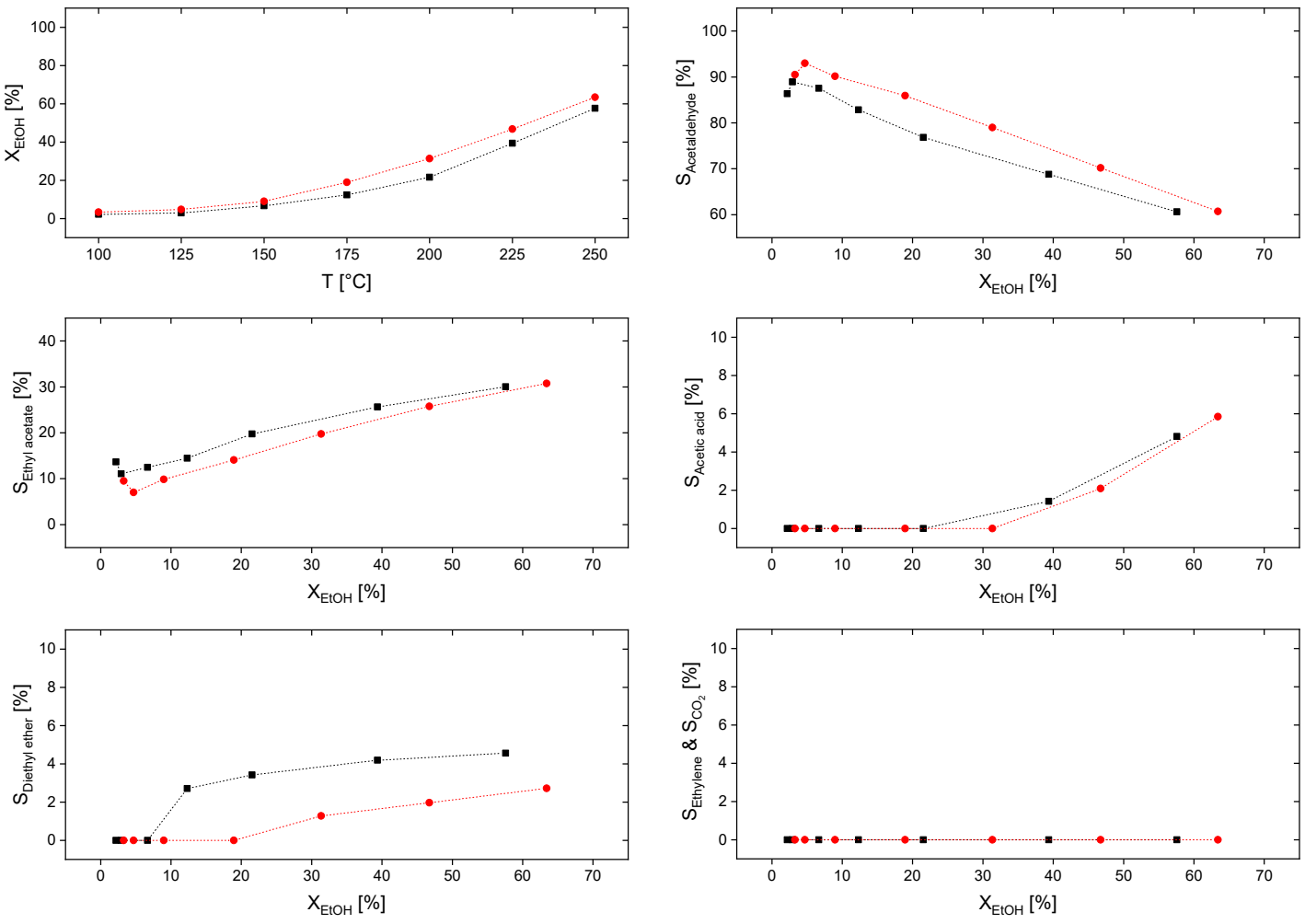

Figure 21. Catalytic performance of the as received (□,□) and the four-day aged (□,□) catalyst tested in a fixed bed tubular reactor

4. Conclusions

A systematic study was conducted to develop a straightforward and reliable method for microreactor coating with a pre-prepared Au/Al_2O_3 catalyst without incorporation of any binders. The catalyst particle size and viscosity of the catalyst slurry were adjusted via ageing. Ageing for four days diminished the average catalyst particle size from 20 to 2 μm which led to a higher viscosity suitable for coating. Therefore, both the catalyst particle size and viscosity of the catalyst slurry played a crucial role in optimizing the coating uniformity. The drying rate and temperature were also decisive in the optimization of the coating uniformity. Stability of the layers was improved by thermal treatment prior to coating. Physico-chemical characterization revealed that ageing of γ-Al_2O_3 for four days has led to minor transformations to bayerite and gibbsite, keeping the crystallinity of the material intact. Such minor alumina transformations did not have a clear effect on the catalytic behavior. A 24 day coating layer stability/durability test was also performed showing its stability in the microchannels. Initial increase in the catalyst activity was likely due to changes in the oxidation state of gold while coking was a reason of minor catalyst deactivation.

Acknowledgements

This work is a part of the activities of Johan Gadolin Process Chemistry Centre (PCC) at Åbo Akademi University. E.B. gratefully acknowledges the financial support from the Graduate School in Chemical Engineering (GSCE) for PhD studies. Academy of Finland is acknowledged for the academy professor grant, 319002 (T. Salmi). The authors would like to thank F. Messerschmidt from the Institute for Micro Process Engineering at the Karlsruhe Institute of Technology (KIT) for analyzing the coated samples via cross sectional SEM.

References

[1] V. Hessel, S. Hardt and H. Löwe, Chemical micro process engineering, Weinheim: WILEY-VCH, 2004.

[2] R. Munirathinam, J. Huskens, W. Verboom, Supported catalysis in continuous-flow microreactors, Adv. Syn. & Catal. 357 (2015) 1093-1123.

[3] S. Born, E. O' Neal, K.F. Jensen, Organic synthesis in small scale continuous flow: flow chemistry, in P. Knochel, G.A, Molander, from Comprehensive Organic synthesis, 9 (2014) 54-93.

[4] S. Hardt, W. Ehrfeld, V. Hessel, K.M. Vanden Bussche, Simulation of heat-transfer enhancement effects in microreactors, in Technical Proceedings of the International

Conference on Modeling and Simulation of Microsystems, San Diego, California, USA, 2000.

[5] E.V. Rebrov, T. Duisters, P. Lo, J. Meuldijk, V. Hessel, Enhancement of the liquid-side mass transfer in a falling film catalytic microreactor by in-channel mixing structures, Ind. Eng. Chem. Res. 51 (2012) 8719-8725.

[6] C.M. Knoesche, Heat transfer and backmixing in microstructured apparatuses, Chemie Ingenieur Technik, 77 (2005) 1720-1722.

[7] M. Saber, J.M. Commenge, L. Falk, Microreactor numbering-up in multi-scale networks for industrial-scale applications: Impact of flow maldistribution on the reactor performances, Chem. Eng. Sci. 65 (2010) 372-379.

[8] B. Sun, J. Jiang, N. Shi, W. Xu, Application of microfluidics technology in chemical engineering for enhanced safety, Process Saf. Prog. 35 (2016) 365-373.

[9] K. Haas-Santo, O. Görke, K. Schubert, J. Fiedler, H. Funke, A microstructure reactor system for the controlled oxidation of hydrogen for possible application in space, in Microreaction Technology, Berlin, Heidelberg, 2001.

[10] T. Illg, A. Knorr, L. Fritzsche, Microreactors- A powerful tool to synthesize peroxycarboxylic esters, Molecules, 21 (2016) 5-21.

[11] Z.Y. Han, W.T. Li, Y.Y. Huang, B. Zheng, Measuring rapid enzymatic kinetics by electrochemical method in droplet-based microfluidic devices with pneumatic valves, Anal. Chem. 81 (2009) 5840-5845.

[12] S. Schwolow, F. Braun, M. Rädle, N. Kockmann, T. Röder, Fast and efficient acquisition of kinetic data in microreactors using in-line Raman analysis, Org. Process Res. Dev. 19 (2015) 1286-1292.

[13] A. Renken, L. Kiwi-Minsker, Microstructured catalytic reactors, Adv. Catal. 53 (2010) 47-122.

[14] A. Tanimu, S. Jaenicke, K. Alhooshani, Heterogeneous catalysis in continuous flow microreactors: A review of methods and applications, Chem. Eng. J. 327 (2017) 792-821.

[15] V. Hessel, G.A. Kolb, J.J. Brandner, Microfabrication for energy generating devices and fuel processors, in: A. Mitsos, P.I. Barton (chapter 7), Microfabricated power generation devices: Design and technology, Wiley-VCH, New York, 2009.

[16] G. Kolb, Review: Microstructured reactors for distributed and renewable production of fuels and electrical energy, Chem, Eng. Process.Process Intensif. 65 (2013) 1-44.

[17] X. Yao, Y. Zhang, L. Du, J. Liu, J. Yao, Review of the applications of microreactors, Renewable Sustainable Energy Rev. 47 (2015) 519-539.

[18] P.L. Suryawanshi, S.P. Gumfekar, B.A. Bhanvase, S.H. Sonawane, M.S. Pimplapure, A review on microreactors: Reactor fabrication, design, and cutting-edge applications, Chemical Engineering Science, 189 (2018) 431-448.

[19] Z. Vajglová, N. Kumar, K. Eränen, M. Peurla, D.Yu. Murzin, T. Salmi, Ethylene oxychlorination over $CuCl_2$/g-Al_2O_3 catalyst in micro- and millistructured reactors, Journal of Catalysis, 364 (2018) 334-344.

[20] Z. Vajglová, R. Hemery, N. Kumar, K. Eränen, M. Peurla, J. Peltonen, J. Wärnå, J. Perez-Ramirez, D.Yu. Murzin, T. Salmi, Kinetics of ceria-catalysed ethene oxychlorination, Journal of Catalysis, 372 (2019) 287-298.

[21] R. Sheldon, I.W.C.E. Arends, G.J. Ten Brink, A. Dijksman, Green, catalytic oxidations of alcohols, Accounts of Chemical Research, 35 (2002) 774-781.

[22] R.A. Sheldon, Recent advances in green catalytic oxidations of alcohols in aqueous media, Catalysis Today, 247 (2014) 4-13.

[23] X. Yao, C. Bai, J. Chen, Y. Li, Efficient and selective green oxidation of alcohols by MOF-derived magnetic nanoparticles as a recoverable catalyst, RSC Advances, 6 (2016) 26921–26928.

[24] E. Behravesh, N. Kumar, Q. Balme, J. Roine, J. Salonen, A. Schukarev, J. P. Mikkola, M. Peurla, A. Aho, K. Eränen, D.Y. Murzin, T. Salmi, Synthesis and characterization of Au nano particles supported catalysts for partial oxidation of ethanol: Influence of

solution pH, Au nanoparticle size, support structure and acidity, J. Catal. 353 (2017) 223-238.

[25] P. Pfeifer, Application of catalysts to metal microreactor systems, in: V. Patel (Ed), Chem. Kin. 2012.

[26] B.S. Flowers, R.L. Hartman, Particle handling techniques in microchemial processes, Challenges, 3 (2012) 194-211.

[27] O.H. Laguna, M. González Castaño, M.A. Centeno, J.A. Odriozola, Microreactors technology for hydrogen purification: Effect of the catalytic layer thickness on CuOx/CeO_2-coated microchannel reactors for the PROX reaction, Chem. Eng. J. 275 (2015) 45-52.

[28] E.V. Rebrov, M.H.J.M. de Croon, J.C. Schouten, Design of a microstructured reactor with integrated heat-exchanger for optimum performance of a highly exothermic reaction, Catal. Today, 69 (2001) 183-192.

[29] S. Zhao, J. Zhang, D. Weng, X. Wu, A method to form well-adhered ɣ-Al_2O_3 layers on FeCrAl metallic supports, Surf. Coat. Technol, 167 (2003) 97-105.

[30] M. Valentini, G. Groppi, C. Cristiani, M. Levi, E. Tronconi, P. Forzatti, The deposition of ɣ-Al_2O_3 layers on ceramic and metallic supports for the preparation of structured catalysts, Catal. Today, 69 (2001) 307-314.

[31] G. Wiessmeier, D. Hnicke, Heterogeneously catalyzed gas-phase hydrogenation of cis,trans,trans-1,5,9-cyclododecatriene on palladium catalysts having regular pore systems, Ind. Eng. Chem. Res. 35 (1996) 4412-4416.

[32] H. Butcher and B.A. Wilhite, Enhancing catalyst effectiveness by increasing catalyst film thickness in coated-wall microreactors: exploiting heat effects in catalytic methane steam micro-reformers, Chem. Eng. Sci. 143 (2016) 47-54.

[33] V. Meille, Reviews on methods to deposit catalyst on structured surfaces, Appl. Catal. Gen. 315 (2006) 1-17.

[34] P. Pfeifer, K. Shubert, M.A. Liauw, G, Emig, PdZn catalysts prepared by washcoating microstructured reactors, Appl. Catal. Gen. 270 (2004) 165-175.

[35] F.J. Echave, O. Sanz, M. Montes, Washcoating of micro-channel reactors with PdZnO catalyst for methanol steam reforming, Appl. Catal. Gen. 474 (2014) 159-167.

[36] L.A. Truter, P.R. Makgwane, B. Zeelie, S. Roberts, W. Böhringer, J.C.Q. Fletcher, Washcoating of H-ZSM-5 zeolite onto steel microreactor plates - Filling the void space between zeolite crystallite agglomerates particles, Chem. Eng. J. 257 (2014) 148-158.

[37] X. Kong, M. Qiu, A. Wang, L. Yang, R. Zhou, Y. Fan, D. Kong, C. Gu, Influence of alumina binders on adhesion and cohesion during preparation of Cu-SAPO-34/monolith catalysts, International Journal of Applied Ceramic Technology, 15 (2018) 1490-1501.

[38] R. Balzarotti, C. Cristiani, L.F. Francis, Combined dip-coating/spin-coating depositions on ceramic honeycomb monoliths for structured catalysts preparation, Catalysis Today,. https://doi.org/10.1016/j.cattod.2019.01.037.

[39] P. Forzatti, D. Ballardini, L. Sighicelli, Preparation and characterization of extruded monolithic ceramic catalysts, Catal. Today, 41 (1998) 87-94.

[40] S. Schmidt, N. Kumar, B. Zhang, K. Eränen, D.Y. Murzin, T. Salmi, Preparation and characterization of alumina-based microreactors for application in methyl chloride synthesis, Ind. Eng. Chem. Res. 51 (2012) 4545-4555.

[41] S. Ivanova, V. Pitchon, C. Petit, H. Herschbach, A. Van Dorsselaer. E. Leize, Preparation of alumina supported gold catalysts: Gold complexes genesis, identification and speciation by mass spectrometry, Appl. Catal. Gen, 298 (2006) 203-210.

[42] D. Dollimore, G.R. Heal, An improved method for the calculation of pore size distribution from adsorption data, J. Appl. Chem. 14 (1964) 109-114.

[43] Powder Diffraction, International Centre for Diffraction Data (ICDD), sets 1-46, 1996.

[44] Inorganic Crystal Structure Database (ICSD), version 2.1.0, 2018. http://www.fizkarlsruhe.de/icsd.html.

[45] D. Kubicka, N. Kumar, P. Mäki-Arvela, M. Tiitta, V. Niemi, T. Salmi, D.Yu. Murzin, Ring opening of decalin over zeolites I. Activity and selectivity of proton-form zeolites, J. Catal. 222 (2004) 65-79.

[46] C.A. Emeis, Determination of integrated molar extinction coefficients for infrared absorption bands of pyridine adsorbed on solid acid catalysts, J. Catal. 141 (1993) 347-354.

[47] J. R. Anderson, Structure of metallic catalysts, Academic Press, London, 1975.

[48] W. Ma, P.W. Brown, Mechanisms of reaction of hydratable aluminas, J. Am. Ceram. Soc. 82 (1999) 453-456.

[49] C. Agrafiotis, A. Tsetsekou, A. Ekonomakou, The effect of particle size on the adhesion properties of oxide washcoats on cordierite honeycombs, J. Mate. Sci. Lett. 18 (1999) 1421-1424.

[50] C. Agrafiotis, A. Tsetsekou, The effect of powder characteristics on washcoat quality. Part 1: Alumina washcoats, J. Eur. Ceram. Soc. 20 (2000) 815-824.

[51] P. Pfeifer, K. Schubert, G. Emig, Preparation of copper catalyst washcoats for methanol steam reforming in microchannels based on nanoparticles, Appl. Catal. Gen. 286 (2005) 175-185.

[52] S. Katheria, G. Deu, D. Kunzru, Washcoating of $Ni/MgAl_2O_4$ catalyst on FeCr alloy monoliths for steam reforming of methane, Energy Fuels, 31 (2017) 3143-3153.

[53] V. Meille, S. Pallier, P. Rodriguez, Reproducibility in the preparation of alumina slurries for washcoat application-Role of temperature and particle size distribution, Colloids Surf. A Physicochem. Eng. Asp. 336 (2009) 104-109.

[54] A. Stefanescu, A.C. van Veen, C. Mirodatos, J.C. Beziat, E. Duval-Brunel, Wall coating optimization for microchannel reactors, Catal. Today, 125 (2007) 16-23.

[55] X. Carrier, E. Marceau, J.F. Lambert, M. Che, Transformations of γ-alumina in aqueous suspensions: 1. Alumina chemical weathering studied as a function of pH, J. Colloid Interface Sci. 308 (2007) 429-439.

[56] G. Lefevre, M. Duc, P. Lepeut, R. Caplain, M. Fedoroff, Hydratio of γ-alumina in water and its effects on surface reactivity, Langmuir, 18 (2002) 7530-7537.

[57] G. Verdes, R. Gout, S. Castet, Thermodynamic properties of the aluminate ion and of bayerite, boehmite, diaspore and gibbsite, Eur. J. Mineral. 4 (1992) 767-792.

[58] C. Cristiani, M. Valentini, M. Merazzi, S. Neglia, P. Forzatti, Effect of ageing time on chemical and rheological evolution in γ-alumina slurries for dip-coating, Catal. Today, 105 (2005) 492-498.

[59] J.M. Mieth, Y.J. Huang, J.A. Schwarz, Experimental procedures to evaluate dissolution, metal ion buffering, and catalytic precursor speciation during catalyst preparation, J. Colloid Interface Sci. 123 (1988) 366-379.

[60] G. Paglia, C.E. Buckley, A.L. Rohl, B.A. Hunter, R.D. Hart, J.V. Hanna, L.T. Byrne, Tetragonal structure model for boehmite-derived γ-alumina, Phys. Rev. B, 68 (2003) 144110-1-144110-11.

[61] R. Rothbauer, F. Zigan, H.Z. O'Daniel, Kristallogr, Kristallgeom, Kristallphys, 125 (1967) 317.

[62] A. Cisar, K. Poulsen, ICDD Grant-in-Aid, Dow Chemical Company, Freeport, TX, USA, 1979.

[63] Z. Zhou, P.J. Scales, D.V. Boger, Chemical and physical control of the rheology of concentrated metal oxide suspensions, Chem. Eng. Sci. 56 (2001) 2901-2920.

[64] H.G. Yang, C.Z. Li, H.C. Gu, T.N. Fang, Rheological behavior of titanium dioxide suspensions, J. Colloid Interface Sci. 236 (2001) 96-103.

[65] J. Yuan, H.H. Murray, The importance of crystal morphology on the viscosity of concentrated suspensions of kaolins, Appl. Clay Sci. 12 (1997) 209-219.

[66] W.H. Boersma, J. Lave, H.N. Stein, Shear thickening (dilatancy) in concentrated dispersions, Am. Inst. Chem. Eng. J. 36 (1990) 321-332.

[67] C. Agrafiotis, A. Tsetsekou, The effect of processing parameters on the properties of γ-alumina washcoats deposited on ceramic honeycombs, J. Mater. Sci. 35 (2000) 951-960.

[68] T. Defraeye, Advanced computational modelling for drying process-A review, Appl. Energy, 131 (2014) 323-344.

[69] V. Novák, P. Kočí, T. Gregor, J.S. Choi, F. Štěpánek, M. Marek, Effect of cavities and cracks on diffusivity in coated catalyst layer, Catal. Today, 216 (2013) 142-149.

[70] R. Zapf, C. Becker-Willinger, K. Berresheim, H. Bolz, H. Gnaser, V. Hessel, G. Kolb, P. Löb, A.K. Pannwitt, A. Ziogas, Detailed characterization of various porous alumina-based catalyst coatings within microchannels and their testing for methanol steam reforming, Chem. Eng. Res. Des. 81 (2003) 721-729.

[71] G. Germani, A. Stefanescu, Y. Schuurman, A.C. van Veen, Preparation and characterization of porous alumina-based catalyst coatings in microchannels, Chem. Eng. Sci. 62 (2007) 5084-5091.

[72] M. Haruta, N. Yamada, T. Kobayashi, S. Iijima, Gold catalysts prepared by coprecipitation for low-temperature oxidation of hydrogen and of carbon monoxide, J. Catal. 115 (1989) 301-309.

[73] S.M. Tembe, G. Patrick, M.S. Scurrell, Acetic acid production by selective oxidation of ethanol using Au catalysts supported on various metal oxide, Gold Bull. 42 (2009) 321-327.

[74] B.S. Gudkov, A.N. Subbotin, V.I. Yakerson, On the phenomena of temperature hysteresis in hydrogenation reactions over heterogeneous catalysts, React. Kin. Catal. Lett. 68 (1999) 125-132.